Dual Frequency Doppler Radars for Indoor Range Estimation: Cramér-Rao Bound Analysis

Pawan Setlur, Moeness Amin, and Fauzia Ahmad
Radar Imaging Lab, Center for Advanced Communications, Villanova University
800 Lancaster Ave, Villanova, PA 19085, USA.
E-mail:{pawan.setlur, moeness.amin, fauzia.ahmad}@villanova.edu

Abstract

Single frequency Doppler radars are effective in distinguishing moving targets from stationary targets, but suffer from inherent range ambiguity. With a dual-frequency operation, a second carrier frequency is utilized to overcome the range ambiguity problem. In urban sensing applications, the dual-frequency approach offers the benefit of reduced complexity, fast computation time, and real time target tracking. We consider a single moving target with three commonly exhibited indoor motion profiles, namely, constant velocity motion, accelerating target motion, and micro-Doppler motion. RF signatures of indoor inanimate objects, such as fans, vibrating machineries, and clock pendulums, are characterized by micro-Doppler motion, whereas animate translation movements produce linear FM Doppler. In this paper, we derive Cramér-Rao bounds (CRB) for the parameters defining indoor target motions under dual-frequency implementations. Experimental data is used to estimate micro-Doppler parameters and to validate the CRBs.

Keywords: Doppler, Cramér-Rao bounds, micro-Doppler, and through-the-wall radar.

I. Introduction

The emerging area of through-the-wall sensing addresses the desire to see inside enclosed structures and behind walls in order to determine building layouts, scene contents, and occupant locations. This capability has merits in a variety of civilian and military applications, as it provides vision into otherwise obscured areas, thereby, facilitating information-gathering and intelligent decision-making [1-4].

Motion detection is a highly desirable feature in many through-the-wall applications, such as firefighters searching for survivors or law-enforcement officers involved in hostage rescue missions. Doppler discrimination of movement from stationary background clutter can be readily used in these applications. Such systems can be classified into zero, one, two, or three dimensional systems [1]. A 0-D system simply provides a go/no-go motion detection capability and, as such, can employ single frequency continuous wave (CW) waveforms for scene interrogation. A 1-D system can provide range to moving targets by employing modulated or pulsed signals. A 2-D system provides both target range and azimuth information, whereas a 3-D system adds the dimension of height to the offerings of a 2-D system. However, the higher level of situational awareness offered by 2-D and 3-D systems is obtained at the expense of increased hardware and software complexity and higher computational load. A 1-D system provides a good compromise between level of situational awareness and cost versus size and weight. This is specifically the case when localizing moving targets is of primary interest.

In this paper, we consider a 1-D system for range-to-motion estimation based on Doppler radars. Single frequency CW radars suffer from range ambiguity [5]. This problem is more pronounced for through-the-wall applications since the carrier frequencies are in the few GHz range due to antenna size and frequency allocation management issues. An additional carrier frequency can be introduced to resolve the uncertainty in range. The two carrier frequencies can be chosen such that the maximum unambiguous range is either equal to or greater than the spatial extent of the urban structure. In this case, the true solution is the one which corresponds to the target inside the enclosed structure. It is noted that other radar techniques, such as the swept frequency, pulse compression etc., can be used to reduce the uncertainty in range [5]. However, the operational logistics and system requirements for through-the-wall operations, such as cost, hardware complexity, and portability, may prohibit the use of such techniques. The dual-frequency approach, although not new, meets all of the above requirements and is likely to emerge as a leading forerunner in modern urban sensing systems [6-9].

We focus on three target motion and range profiles, namely, linear translation, acceleration, and the micro-Doppler (MD) motions that are commonly encountered in urban sensing applications. For example,

the swinging of the arms and the legs of a person during walking can be modeled as micro-Doppler, whereas the gross motion of the torso can be represented by translation. We develop Cramér-Rao bounds (CRBs) for the parameters corresponding to the aforementioned three indoor motion profiles. We provide the CRB for the range estimate in addition to motion speed, harmonic frequency, and chirp parameters. Specifically, we show that the dual frequency approach increases the Fisher information compared to a single frequency operation and, therefore, lowers the CRBs [10]. In the analysis, the radar aspect angle θ is incorporated into the general CRB derivations. When the aspect angle is assumed unknown, the FIM becomes singular, rendering the parameters non-identifiable. It is noted that the main contribution of the paper is the derivation of the CRBs, and no estimation technique is advocated here. For MD motion, we use experimental data to estimate micro-Doppler parameters and to validate the CRBs. We employ suboptimal techniques that make use of the inherent impulsive structure of the spectrum of the returns to estimate some of the parameters in the MD model [10]. Maximum Likelihood optimal estimator for MD motion profile is presented in [10].

A brief outline of the paper is as follows. In Section II, the signal model is introduced along with the governing range equations for the three motion profiles. In Section III, a generic derivation of the CRB is presented, incorporating the nuisance parameters, and subsequently the CRBs of the three motion profiles are derived. Supporting simulation and experimental results are provided in Section IV. Section V contains the conclusions.

II. General Signal Model

Below, we briefly discuss the range ambiguity problem, and introduce the motivation for adopting carrier frequency diversity in CW radar for range estimation.

A. Range Ambiguity in Dual-frequency Radar

For a dual frequency radar employing two known carrier frequencies f_1 and f_2, the baseband signal returns due to a single moving target are expressed as,

$$\varphi_1(nT_s) = 4\pi f_1 R(nT_s)/c\ ,\ \varphi_2(nT_s) = 4\pi f_2 R(nT_s)/c \tag{1}$$

where T_s is the sampling period, $R(nT_s)$ is the range of the target at sample n, and c is the speed of light in free space. Dropping T_s in the phase and range notations for convenience, and without considering phase wrapping, the range of the target is given by [6]

$$R(n) = \frac{c(\varphi_2(n) - \varphi_1(n))}{4\pi(f_2 - f_1)} \tag{2}$$

In reality, however, phase observations are wrapped within the $[0, 2\pi)$ range. Therefore, the true phase can be expressed as

$$\phi^{(true)}(n) = \phi_2(n) - \phi_1(n) + 2m\pi, \tag{3a}$$

where m is an unknown integer. Accordingly, the range estimate is subject to range ambiguity [7], i.e,

$$R(n) = \frac{c[\phi_2(n) - \phi_1(n)]}{4\pi(f_2 - f_1)} + \frac{cm}{2(f_2 - f_1)}. \tag{3b}$$

The second term in the above equation induces ambiguity in range. For the same phase difference, the range can assume infinite values separated by

$$R_u = c / (2(f_2 - f_1)) \tag{3c}$$

which is referred to as the maximum unambiguous range. From the above equation, R_u is inversely proportional to the difference of the carrier frequencies. Consider a single frequency Doppler radar operating at $f_1 = 1$ GHz. In this case, $R_u = c / 2f_1 = 15$ cm. For dual frequency operation at $f_1 = 1$ GHz, and $f_2 = 1.01$ GHz, $R_u = 15$ m, according to (3a). The increase in R_u from 15 cm to 15 m is sufficient for target location in rooms and small buildings. The other multiple range solutions given by (2), and (3b) are simply rejected since they do not fall within the spatial extent of the urban structure. In the following sections, we, therefore, assume $m = 0$, for simplicity. By choosing closely separated carrier frequencies, any maximum unambiguous range can be achieved. Coherent phase estimation may, however, be compromised if the frequency difference is too small to overcome noise effects and frequency drifts in down conversions [11]. Performance analysis of the dual-frequency radar in the presence of noise and frequency drifts is provided in [12]-[13].

It is noted that in the presence of multiple moving targets, the phase extracted from the radar returns cannot be used for range estimation of each target separately. This is because the phase terms corresponding to different targets are superimposed and cannot be separated in the time domain. This drawback of the dual-frequency scheme can be overcome provided that the target Doppler signatures are separable in the frequency or the time-frequency (TF) domain [14]. With the extraction of the phase of the individual targets in the Doppler domain, (2) can then be used to obtain the corresponding target range. Likewise for multipath which is similar to multiple targets the same procedure can be applied, provided they are separable in the frequency or time-frequency domain.

B. Signal Model for CRB Derivation

For a dual frequency radar employing two known carrier frequencies f_1 and f_2, the baseband signal returns due to a single moving target are expressed as,

$$\begin{aligned} x_1(n) &= x_1(nT_s) = (\rho_1 + h_1(n;\boldsymbol{\psi}))\exp\left(j\frac{4\pi f_1 R(n)}{c}\right) + v_1(n) = s_1(n) + v_1(n) \\ x_2(n) &= x_2(nT_s) = (\rho_2 + h_2(n;\boldsymbol{\psi}))\exp\left(j\frac{4\pi f_2 R(n)}{c}\right) + v_2(n) = s_2(n) + v_2(n) \\ &\{n \mid n \in Z^+, n = 0,1,2,3\ldots N-1\} \end{aligned} \tag{4}$$

where ρ_i is the amplitude of the return at frequency $f_i, i = 1,2$. The scalar function $h_i(n;\boldsymbol{\psi})$, dependent on both the sample index n and a vector $\boldsymbol{\psi}$ of desired parameters, is added to represent possible cyclic amplitude fluctuations for the MD model. It is noted that for the case of constant Doppler and accelerating target motion profiles, $h_i(n;\boldsymbol{\psi}) = 0,$ since for these targets the radar cross section (RCS) can be assumed constant for a relatively small time on target. Z^+ is the domain of positive integers. The two noise sequences, corresponding to the two frequencies of operation, over the observation period N, are complex additive white Gaussian noise (AWGN) and uncorrelated, i.e., $v_1(n) = v_1(nT_s) \sim CN(0,\sigma_1^2)$, $v_2(n) = v_2(nT_s) \sim CN(0,\sigma_2^2)$, $E\{v_1(n)v_2^*(n)\} = 0,$ where σ_1^2 and σ_2^2 represent the noise variance for the two frequencies, respectively and '$*$' is the complex conjugate operator. To aid in the derivation, we

vectorize the observations and describe the signal returns by a joint probability density function (pdf). The received signals at the two frequencies are appended to form a long vector,

$$\mathbf{x} = \mathbf{s} + \mathbf{v} = \left[x_1(0), x_1(1), x_1(2)....x_1(N-1), x_2(0), x_2(1).....x_2(N-1)\right]^T = [\mathbf{x_1} \quad \mathbf{x_2}]^T \tag{5}$$

where

$$\begin{aligned} \mathbf{s} &= [s_1(0), s_1(1), s_1(2)....s_1(N-1), s_2(0), s_2(1).....s_2(N-1)]^T = [\mathbf{s_1} \quad \mathbf{s_2}]^T \\ \mathbf{v} &= [v_1(0), v_1(1), v_1(2)....v_1(N-1), v_2(0), v_2(1)...v_2(N-1)]^T = [\mathbf{v_1} \quad \mathbf{v_2}]^T \end{aligned} \tag{6}$$

The mean and covariance matrix of $\mathbf{x}$ are given by

$$E\{\mathbf{x}\} = \boldsymbol{\mu} = [\mathbf{s_1} \quad \mathbf{s_2}]^T, \quad E\{(\mathbf{x}-\boldsymbol{\mu})(\mathbf{x}-\boldsymbol{\mu})^H\} = \mathbf{C} = \begin{bmatrix} \sigma_1^2\mathbf{I} & \mathbf{0}_{N\times N} \\ \mathbf{0}_{N\times N} & \sigma_2^2\mathbf{I} \end{bmatrix} \tag{7}$$

The joint pdf of the data, assuming a multivariate complex Gaussian distribution, is

$$p(\mathbf{x};\mathbf{s}) = \frac{1}{\pi^{2N}\det(\mathbf{C})}\exp(-(\mathbf{x}-\boldsymbol{\mu})^H\mathbf{C}^{-1}(\mathbf{x}-\boldsymbol{\mu})) \tag{8}$$

1) Constant Doppler Frequency

For the constant Doppler frequency model, the target range is parameterized as,

$$R(n) = R_o + v\cos(\theta)n, \quad \theta \in (-\pi/2, \pi/2) \tag{9}$$

where R_o is the initial range of the target at time $n = 0$. The discrete velocity v of the target is its actual velocity multiplied by the sampling period. The parameter θ is the viewing, or aspect, angle of the radar with respect to the target. In other words, the component $v\cos(\theta)$ is the identifiable Doppler component registered by the radar system. Inserting (9) into (4), it is clear that the constant Doppler model is analogous to the sinusoidal parameter estimation [15, 16]. Hence, the identifiability criteria of the parameters are similar to the traditional single frequency estimation problem. However, some details must be added. The identifiability criteria are developed by putting $\theta = 0$ in (9) because for any other value of θ in the defined range, the criteria are valid. The terms $2f_1v/c$ and $2f_2v/c$ in the phase of the signal returns are the Doppler frequencies, analogous to the frequencies (radian/s) in the sinusoidal parameter estimation problem. Hence, for v to be identifiable, $-0.5 \le 2f_1v/c < 0.5$ and $-0.5 \le 2f_2v/c < 0.5$ [15].

Since we have assumed $f_2 > f_1$ implicitly, $-c/4f_2 \le v < c/4f_2$ represents the bounds on the positive and negative Doppler, respectively. For example, if $f_2 = 1$ GHz, then the discrete velocity is constrained to a maximum of 0.075, assuming a nominal sampling frequency of 100Hz and the analog velocity is 7.5 m/s. It is noted that indoor animate moving targets such as humans and pets, do not assume such high velocities. Typically, in indoor settings, we expect analog velocities below 1m/s which allows the sampling frequency to be reduced to approximately 15 Hz. The terms $4\pi f_1 R_o/c$ and $4\pi f_2 R_o/c$ represent the phase in the sinusoidal parameter estimation model. Clearly, R_o can be uniquely estimated if the maximum unambiguous range is larger than the building extent, as determined by (3c). For this motion profile, as mentioned earlier, we use $h_i(n;\boldsymbol{\psi}) = 0,$ since the RCS is assumed to be constant.

2) Micro-Doppler (MD)

The range for this motion profile is parameterized as [17],

$$R(n) = R_o + d\cos(\theta)\cos(\omega_o n - \varphi_o), \quad (d, \omega_o) \neq 0, \quad \theta \in (-\pi/2, \pi/2) \tag{10}$$

In the above equation, the parameter ω_o is the discrete version of the rotational or the vibrational frequency. The parameter $d\cos(\theta)$ is the maximum displacement from the initial range R_o along the radar's line of sight (LOS). For the specific case of rotation, $2d\cos(\theta)$ represents the diameter of the circular trajectory in the direction of the LOS. The parameter φ_o denotes the initial phase of the MD motion. The MD signal returns represent the traditional sinusoidal FM model [10, 11], and are obtained by substituting (10) in (4). It is noted that the sinusoidal FM model is a good fit for motion profiles of indoor inanimate objects, such as fans, vibrating machineries, and clock pendulums. For the more complicated human motion, the sinusoidal FM model is a rough approximation to the swinging of the arms and the legs during walking.

The MD model can be further decomposed into vibration and rotation models based on the scalar function $h_i(n;\boldsymbol{\psi})$. For typical indoor targets undergoing pure vibration (i.e. the target moves back and forth), the displacements are small relative to the target range, especially for longer radar standoff distances from the

wall, and the RCS is considered to be constant, i.e., $h_i(n;\boldsymbol{\psi}) = 0$. On the other hand, for a rotating target, a fixed-location radar observes different elevation aspects of the target, thereby inducing a cyclic amplitude modulation in the radar returns. These amplitude fluctuations are indeed dependent on the target geometry. In this case, the scalar function $h_i(n;\boldsymbol{\psi})$ can be modeled as

$$h_i(n;\boldsymbol{\psi}) = \Delta\rho_i \cos(\omega_o n - \phi_i) \tag{11}$$

where the parameter $\Delta\rho_i$ represents the maximum deviation from the nominal amplitude ρ_i, whereas the parameter $\phi_i \in [0, 2\pi)$ represents the phase at time $n = 0$. As an example, consider a rotating fan with one blade, at one extreme instant of time the tip of the blade is seen representing a near zero RCS, whereas at another extreme time instant, the entire length of the blade is seen by the radar representing a maximum RCS. The cyclic amplitude modulations will be demonstrated experimentally in the simulations section and are in agreement with the model in (11).

The identifiability criteria for MD signals are developed by substituting $\theta = 0$ in (10). For the variable R_o, this case is identical to the case of constant Doppler. However, it is not straightforward to derive the parameter identifiability criteria for the rest of the parameters using the time domain model alone, as was the case in the constant Doppler model. We use the Fourier transform to aid in the derivation and to shed more light on the identifiability bounds and the discrete parameterization in the MD model. The noise free MD returns are given by,

$$s_i(n) = (\rho_i + h_i(n;\boldsymbol{\psi})) \exp\left(j\frac{4\pi f_i R_o}{c} + j\frac{4\pi f_i d\cos(\omega_o n - \varphi_o)}{c} \right), \ \forall i = 1,2 \tag{12}$$

Let $J_k(\cdot)$ be the k^{th} order Bessel function of the first kind. Accordingly [18, 19],

$$\exp\left(j\frac{4\pi f_i d}{c}\cos(\omega_o n - \varphi_o) \right) = \sum_{k=-\infty}^{\infty} j^k \exp(jk(\omega_o n - \varphi_o)) J_k\left(\frac{4\pi f_i d}{c} \right) \tag{13}$$

Using (12) and the Fourier representation of (13), and ignoring $h_i(n;\boldsymbol{\psi})$, as it does not affect identifiability, we obtain

$$S_i(e^{j\omega}) = \rho_i \exp\left(j\frac{4\pi f_i R_o}{c} \right) \sum_{k=-\infty}^{\infty} j^k \delta(\omega - k\omega_o) \exp(-jk\varphi_o) J_k\left(\frac{4\pi f_i d}{c} \right), \ \forall i = 1,2 \tag{14}$$

As in traditional multiple sinusoidal parameter estimation, for the frequencies to be identifiable, they must lie in the interval $[-\pi, \pi)$. This condition, which translates in the underlying case to $-\pi \le k\omega_o < \pi, \ \forall k, \ k \in Z,$ cannot be imposed, since there is an infinite number of harmonics. Moreover, it is clear from (14) that the signal is not analytic due to the presence of harmonics in the negative frequencies. However, it is well known that the Bessel functions decrease rapidly with k. Therefore, we impose the following two assumptions to derive the identifiability constraints: 1) Most of the energy in the signal can be represented by a finite number of harmonics; say $K \in Z$, 2) The Nyquist theorem is satisfied. Assumption 1 implies that the Fourier transform in (14) can be replaced by

$$S_i(e^{j\omega}) = \rho_i \exp\left(j\frac{4\pi f_i R_o}{c} \right) \sum_{k=-K}^{K} j^k \delta(\omega - k\omega_o) \exp(-jk\varphi_o) J_k\left(\frac{4\pi f_i d}{c} \right), \ \forall i = 1,2 \tag{15}$$

Assumption 2 then implies that $-\pi \le k\omega_o < \pi, \ \forall k, \ -K \le k \le K$ in order to avoid aliasing of the K harmonics. Since negative vibrational and rotational frequencies have no physical meaning, it is straightforward to note that from the above assumptions $\omega_o \in (0, \ \pi)$. Furthermore, since the harmonics are symmetric about DC, and knowing *a priori* that an MD target is present, it is sufficient to identify the first harmonic corresponding to $k = \pm 1$, i.e., $|\omega_o| < \pi$. The criterion $0 \le \varphi_o < 2\pi$ is chosen for identifying φ_o. Surprisingly, the identifiability criteria are similar, although not identical, to the case of sinusoidal parameter estimation. However, the bounds on ω_o and φ_o are carrier independent, unlike the constant Doppler case, where the velocity bound was constrained by the higher carrier frequency, f_2.

The Bessel functions take arguments $4\pi f_i d/c$. Therefore, any real argument, excluding zero, is valid because $J_k(0) = 0, \ \forall k \ne 0$. Since negative values of the maximum displacement, d, have no physical meaning, then $d > 0$. Moreover, in traditional sinusoidal FM, the argument $4\pi f_i d/c$ is analogous to the modulation index [11], which is strictly real and positive. Therefore, $0 < d < \infty$. It is

important to note, however, that it is impractical to constrain the initial range of the target to be within the maximum unambiguous range, while allowing the maximum displacement to be infinite. Therefore, to be consistent, we impose the criterion for d as $0 < d \le c/4(f_2 - f_1) = R_u/2$.

It is noted that typical indoor MD targets, such as rotating fans, pendulums, etc, are essentially narrowband FM (NBFM). For example, consider the motion of a human, the maximum displacement of either the arm or the leg is much less than a meter, and for a carrier in the low GHz range, the bandwidth is typically a few Hz. In the case of an indoor rotating fan, the received signal bandwidth is proportional to the length of the fan's blade, and is clearly a few Hz for such carrier frequencies.

3) Accelerating Target

The range for this motion profile is given by,

$$R(n) = R_o + \cos(\theta)(\alpha n + \beta n^2), \quad \theta \in (-\pi/2, \pi/2) \tag{16}$$

where the parameters α and β represent the initial velocity and half the acceleration (or deceleration) of the target, respectively. As before, R_o is the initial range of the target and its identifiability is identical to the constant Doppler case. Substituting (16) in (4), we obtain the desired signal returns for the accelerating target. It is clear that an accelerating target represents a linear chirp, or a second order Polynomial-phase signal (PPS) [20]. The identifiability criteria are developed by putting $\theta = 0$ in (16). The model is similar to the chirp parameter estimation model, albeit a few differences in identifiability [21]. The terms $4\pi f_i \alpha/c$ and $4\pi f_i \beta/c \quad \forall i,\ i = 1,2$ represent the frequency and chirp rate in the chirp parameter estimation model, respectively. Hence for identifiability, along with the fact that $f_2 > f_1$, we must have $-c/4f_2 \le \alpha < c/4f_2$ and $-c/8f_2 \le \beta < c/8f_2$, which are carrier frequency dependent. It is noted that the bounds are for the discretized versions of the parameters. For this motion profile, $h_i(n;\boldsymbol{\psi}) = 0$.

We note that in indoor environments, the above three motion profiles can occur individually or in

combination. While a rotating fan or a clock pendulum will exhibit purely MD motion, the motion profile of a human walking can be predominantly modeled as a combination of translational and MD components. In this paper, however, we focus on three "stand-alone" motion profiles, namely, translation, MD and acceleration individually. Combinations of these motions are not considered.

III. Cramér Rao Bounds

In this section, we derive the CRB for the three motion profiles discussed previously. The parameter θ is assumed known. In Appendix-A, we show that if θ is unknown, then the FIM becomes singular. We begin with the generalized CRB derivation, taking into account the effect of the nuisance parameters. The parameter vector including the nuisance parameters is denoted by $\boldsymbol{\eta} = [\boldsymbol{\psi}^T, \rho_1, \rho_2, \sigma_1^2, \sigma_2^2]^T_{(p+4)\times 1}$, where $\boldsymbol{\psi} = [\psi_1, \psi_2, \psi_3 ... \psi_p]^T$. The parameters ψ_k, $1 \le k \le p$ are the p desired parameters, some of which are present purely in the phase of the signal returns. In general, the range is a function of both n and $\boldsymbol{\psi}$, i.e. $R(n) = R(n; \boldsymbol{\psi})$. For a complex Gaussian vector $\mathbf{x}$, with a covariance matrix $\mathbf{C}$, defined in (7), the Fisher information elements are expressed as [22],

$$[\mathbf{F}]_{qr} = \mathrm{Tr}\left[\mathbf{C}^{-1} \frac{\partial \mathbf{C}}{\partial \eta_q} \mathbf{C}^{-1} \frac{\partial \mathbf{C}}{\partial \eta_r} \right] + 2\,\mathrm{Re}\left\{ \frac{\partial \mathbf{s}}{\partial \eta_q}^H \mathbf{C}^{-1} \frac{\partial \mathbf{s}}{\partial \eta_r} \right\}, \quad 1 \le (q,r) \le p+4 \tag{17}$$

where $\mathbf{s} = [\mathbf{s_1} \quad \mathbf{s_2}]^T = \left[(\boldsymbol{\rho}_1 + \mathbf{h}_1(\boldsymbol{\psi})) \circ \exp\left(j \frac{4\pi f_1}{c} \mathbf{R}(\boldsymbol{\psi}) \right) \quad (\boldsymbol{\rho}_2 + \mathbf{h}_2(\boldsymbol{\psi})) \circ \exp\left(j \frac{4\pi f_2}{c} \mathbf{R}(\boldsymbol{\psi}) \right) \right]^T$ with the exponential taken elementwise, $\mathbf{R}(\boldsymbol{\psi})$ and $\boldsymbol{\rho}_i + \mathbf{h}_i(\boldsymbol{\psi})$ are $1 \times N$ row vectors, whose n^{th} elements are $R(n; \boldsymbol{\psi})$ and $\rho_i + h_i(n; \boldsymbol{\psi}), i = 1, 2$ respectively. That is, the dependency on n is suppressed. The operator '$\circ$' denotes the Hadamard product or element wise multiplication. Following the work of [23], and using the vector differential operator, we obtain

$$\frac{\partial \mathbf{s}}{\partial \boldsymbol{\eta}^T} = \begin{bmatrix} \mathbf{s_1} \\ \mathbf{s_2} \end{bmatrix} \begin{bmatrix} \frac{\partial}{\partial \boldsymbol{\psi}^T} & \frac{\partial}{\partial \rho_1} & \frac{\partial}{\partial \rho_2} & \frac{\partial}{\partial \sigma_1^2} & \frac{\partial}{\partial \sigma_2^2} \end{bmatrix}$$

$$= \left[\begin{bmatrix} \frac{\partial \mathbf{h}_1(\boldsymbol{\psi})}{\partial \boldsymbol{\psi}^T} \\ \frac{\partial \mathbf{h}_2(\boldsymbol{\psi})}{\partial \boldsymbol{\psi}^T} \end{bmatrix} \bullet \begin{bmatrix} \exp\left(\frac{j4\pi f_1 \mathbf{R}(\boldsymbol{\psi})}{c} \right) \\ \exp\left(\frac{j4\pi f_2 \mathbf{R}(\boldsymbol{\psi})}{c} \right) \end{bmatrix} + \begin{bmatrix} \frac{4\pi f_1}{c} \frac{\partial \mathbf{R}(\boldsymbol{\psi})}{\partial \boldsymbol{\psi}^T} \\ \frac{4\pi f_2}{c} \frac{\partial \mathbf{R}(\boldsymbol{\psi})}{\partial \boldsymbol{\psi}^T} \end{bmatrix} \bullet j\mathbf{s} \quad \frac{\partial \mathbf{s}}{\partial \eta_2} \quad \frac{\partial \mathbf{s}}{\partial \eta_3} \quad \mathbf{0}_{2N\times 1} \quad \mathbf{0}_{2N\times 1} \right]_{2N\times(p+4)} \tag{18}$$

$$\frac{\partial \mathbf{s}}{\partial \eta_2} := \begin{bmatrix} (\boldsymbol{\rho}_1 + \mathbf{h}_1(\boldsymbol{\psi}))^{T\circ -1} \\ \mathbf{0}_{N\times 1} \end{bmatrix} \circ \mathbf{s}, \quad \frac{\partial \mathbf{s}}{\partial \eta_3} := \begin{bmatrix} \mathbf{0}_{N\times 1} \\ (\boldsymbol{\rho}_2 + \mathbf{h}_2(\boldsymbol{\psi}))^{T\circ -1} \end{bmatrix} \circ \mathbf{s}$$

where '$\bullet$' denotes the generalized Hadamard product[1], and '$(\cdot)^{\circ -1}$' denotes the Hadamard division of a vector or a matrix, i.e. if $\mathbf{x} = [x_1 x_2 ... x_N]$, $\mathbf{x}^{\circ -1} = [1/x_1, 1/x_2 ... 1/x_N]$.. In (17), the argument of the trace operator is zero except that which corresponds to the Fisher information of the noise nuisance parameters namely, σ_i^2, $i = 1, 2$. Partitioning the FIM,

$$\mathbf{F} = \begin{bmatrix} \mathbf{F}_{11} & \mathbf{F}_{12} \\ \mathbf{F}_{21} & \mathbf{F}_{22} \end{bmatrix} \tag{19}$$

The desired CRBs reside on the diagonal of the inverse Schur complement of $\mathbf{F}$, with respect to $\mathbf{F}_{22}$,

$$CRB(\boldsymbol{\psi}) = [(\mathbf{F}_{11} - \mathbf{F}_{12}\mathbf{F}_{22}^{-1}\mathbf{F}_{21})^{-1}]_{qq} \tag{20}$$

Using (18)-(20), it can be readily shown that

$$\mathbf{F}_{11} = 2\sum_{i=1}^{2} \frac{1}{\sigma_i^2} \left(\frac{\partial \mathbf{h}_i(\boldsymbol{\psi})}{\partial \boldsymbol{\psi}^T} \right)^T \frac{\partial \mathbf{h}_i(\boldsymbol{\psi})}{\partial \boldsymbol{\psi}^T}$$
$$+ \frac{32\pi^2}{c^2} \sum_{i=1}^{2} \frac{f_i^2}{\sigma_i^2} \left((\boldsymbol{\rho}_i + \mathbf{h}_i(\boldsymbol{\psi})) \bullet \frac{\partial \mathbf{R}(\boldsymbol{\psi})}{\partial \boldsymbol{\psi}^T} \right)^T \left((\boldsymbol{\rho}_i + \mathbf{h}_i(\boldsymbol{\psi})) \bullet \frac{\partial \mathbf{R}(\boldsymbol{\psi})}{\partial \boldsymbol{\psi}^T} \right) \tag{21}$$
$$\mathbf{F}_{12} = \mathbf{F}_{21}^T = [\mathbf{0}_p \quad \mathbf{0}_p \quad \mathbf{0}_p \quad \mathbf{0}_p]$$
$$\mathbf{F}_{22} = Diag\left[2N/\sigma_1^2 \quad 2N/\sigma_2^2 \quad N/\sigma_1^4 \quad N/\sigma_2^4 \right]$$

[1] For a matrix $\mathbf{A} \in C^{M\times N} = [\mathbf{a}_1 \, \mathbf{a}_2 .... \mathbf{a}_N]$ and vector $\mathbf{x} \in C^{M\times 1}$ $\mathbf{A} \bullet \mathbf{x} \in C^{M\times N} := [\mathbf{a}_1 \circ \mathbf{x} \;\; \mathbf{a}_2 \circ \mathbf{x} ..... \mathbf{a}_N \circ \mathbf{x}] := \mathbf{x} \bullet \mathbf{A}$

where $Diag[\cdot]$ is a diagonal matrix with entries as given in the brackets and the vector $\mathbf{1}_{N\times 1}$ is the row vector of size N having entries all equal to one. Similarly, the vector $\mathbf{0}_p$ is the column vector of size p, having all zero entries. The CRB of the desired parameters is then expressed in a compact form as

$$CRB([\boldsymbol{\psi}]_q) = \left[\mathbf{F}_{11}^{-1}\right]_{qq} \tag{22}$$

From (22), the CRBs for the desired parameters are completely decoupled from those of the nuisance parameters. The decoupling in (22) indicates that the variance of the range parameters are insensitive to the knowledge, or the information brought in by the estimation of the nuisance parameters, i.e. they are unaffected whether the nuisance parameters are known or unknown [22]. From matrix $\mathbf{F}_{11}$ in (21), we observe that the scalar multiplier terms arise as a result of the carrier diversity, implied by the dual frequency operation, and therefore have an additive effect on the net Fisher information. It yields lower CRBs, when compared to the no diversity (single carrier frequency) case. In fact, the scalar term $32\pi^2(f_1^2/\sigma_1^2 + f_2^2\sigma_2^2)/c^2$ indicates that the CRBs are the lowest when $f_1 = f_2 = 0,$ in which case, $R_u = \infty.$ However, this is a trivial case, as diversity ceases to exist. In general, since the FIM elements are a function of the squared values of f_1 and $f_2,$ lower CRBs are achieved when higher carrier frequencies are chosen. The effect of the SNRs on the CRBs is straightforward to analyze. The addition of Fisher information is explored in greater detail in the following subsections. In the ensuing analysis, we derive the FIM elements for the desired parameters.

A. Constant Doppler CRB

In this case, the parameter vector is $\boldsymbol{\psi} = \begin{bmatrix} R_o & v \end{bmatrix}^T$. Substituting (9) in (21) for the constant Doppler range profile, we obtain the corresponding FIM. In order to make the CRB analysis more generic, we introduce the parameters, $\chi := f_2/f_1,$ and $\psi' := \sigma_1^2/\sigma_2^2$. It can be readily shown that for a single frequency radar employing carrier f_1, the FIM, $\mathbf{F}_{f_1},$ and its inverse are, respectively, given by [10]

$$\mathbf{F}_{f_1} = \frac{32\pi^2\rho_1^2 f_1^2}{c^2\sigma_1^2}\begin{bmatrix} N & \frac{N(N-1)\cos(\theta)}{2} \\ \frac{N(N-1)\cos(\theta)}{2} & \frac{N(N-1)(2N-1)\cos^2(\theta)}{6} \end{bmatrix} \tag{23}$$

$$\mathbf{F}_{f_1}^{-1} = \frac{c^2\sigma_1^2}{\mathrm{K}f_1^2\rho_1^2}\begin{bmatrix} \frac{2(2N-1)}{N(N+1)} & \frac{-6}{\cos(\theta)N(N+1)} \\ \frac{-6}{\cos(\theta)N(N+1)} & \frac{12}{\cos^2(\theta)N(N^2-1)} \end{bmatrix} \tag{24}$$

where $\mathrm{K} = 32\pi^2$ is a constant. However, for the proposed dual frequency scheme, the FIM is given by

$$\mathbf{F} = \frac{32\pi^2 f_1^2}{c^2\sigma_1^2}(\rho_1^2 + \rho_2^2\chi^2\psi')\begin{bmatrix} N & \frac{N(N-1)\cos(\theta)}{2} \\ \frac{N(N-1)\cos(\theta)}{2} & \frac{\cos^2(\theta)N(N-1)(2N-1)}{6} \end{bmatrix} \tag{25}$$

$$\mathbf{F}^{-1} = \frac{c^2\sigma_1^2}{\mathrm{K}(\rho_1^2 + \rho_2^2\chi^2\psi')}\begin{bmatrix} \frac{2(2N-1)}{N(N+1)} & \frac{-6}{\cos(\theta)N(N+1)} \\ \frac{-6}{\cos(\theta)N(N+1)} & \frac{12}{\cos^2(\theta)N(N^2-1)} \end{bmatrix} \tag{26}$$

It is clear from (23) and (25) that the Fisher information for the dual frequency scheme can be written as,

$$\mathbf{F} = \mathbf{F}_{f_1} + \mathbf{F}_{f_2} \tag{27}$$

The diagonal elements in (26) represent the CRBs for the initial range and velocity, respectively. It is evident from the scalar matrix multiplicative factor in (24) and (26) that the CRBs for both the initial range and velocity for the dual frequency case consistently assume smaller values as compared to their counterparts in single frequency operation. Hence, carrier frequency diversity lowers the CRBs for the range parameters. In (26), the matrix elements containing N characterize the temporal diversity in the Fisher information, whereas the scalar multiplier, containing the SNR terms and carriers, represents the carrier diversity in the Fisher information. Hence, the temporal diversity factor is identical for both frequencies, whereas the diversity induced by the carriers is different. If $\chi \approx 1$, and $\psi' = 1$, with $\rho_i \approx \rho, i = 1,2,$ then the carrier frequencies are closely separated and the SNR corresponding to the two frequencies are equal. In this case, the net Fisher information is simply $2\mathbf{F}_{f_1}$ and the CRB are then

$0.5CRB(\boldsymbol{\psi})_{f_1}$, where $CRB(\boldsymbol{\psi})_{f_1}$ is the CRB of the parameter vector $\boldsymbol{\psi}$, associated with the single frequency f_1.

B. Micro-Doppler CRB

The derivation of the CRBs for the MD motion profile is different from that presented in [24], which uses a hybrid combination of PPS and MD signals. The results on the FIM elements presented in [24] are a special case of those presented here and do not provide closed form expressions of the FIM elements for MD signals, neither do they include the aspect angle and range parameters in the employed radar model. Since the frequency diversity appends the individual fisher information regardless of the motion profile, as shown in (27), we can simplify notation by suppressing the terms involving the carrier frequencies and noise variances, i.e., $\varepsilon_{1i} = 2/\sigma_i^2, \forall i = 1,2$ and $\varepsilon_{2i} = 16\pi^2 f_i^2 \varepsilon_{1i} \big/ c^2$.

1) MD Fisher information

In this case, the parameter vector is $\boldsymbol{\psi} = [R_o \quad d \quad \omega_o \quad \varphi_o \quad \Delta\rho \quad \phi]^T$. The FIM can be derived from the general expression (21) using the range equation (10). It is straightforward to show that

$$F_{R_oR_o} = \sum_{i=1}^{2}\sum_{n=0}^{N-1} \varepsilon_{2i}(\rho_i + \Delta\rho_i \cos(\omega_o n - \phi_i))^2 \tag{28}$$

$$F_{R_od} = \cos(\theta)\sum_{i=1}^{2}\sum_{n=0}^{N-1} \varepsilon_{2i}(\rho_i + \Delta\rho_i \cos(\omega_o n - \phi_i))^2 \cos(\omega_o n - \varphi_o) \tag{29}$$

$$F_{R_o\omega_o} = -\cos(\theta)\sum_{i=1}^{2}\sum_{n=0}^{N-1} \varepsilon_{2i}(\rho_i + \Delta\rho_i \cos(\omega_o n - \phi_i))^2 dn \sin(\omega_o n - \varphi_o) \tag{30}$$

$$F_{R_o\varphi_o} = \cos(\theta)\sum_{i=1}^{2}\sum_{n=0}^{N-1} \varepsilon_{2i}(\rho_i + \Delta\rho_i \cos(\omega_o n - \phi_i))^2 d \sin(\omega_o n - \varphi_o) \tag{31}$$

$$F_{R_o\Delta\rho_i} = 0,\ F_{R_o\phi_i} = 0,\ \ F_{d\Delta\rho_i} = 0,\ F_{d\phi_i} = 0 \tag{32}$$

$$F_{dd} = \cos^2(\theta)\sum_{i=1}^{2}\sum_{n=0}^{N-1} \varepsilon_{2i}(\rho_i + \Delta\rho_i \cos(\omega_o n - \phi_i))^2 \cos^2(\omega_o n - \varphi_o) \tag{33}$$

$$F_{d\omega_o} = -\cos^2(\theta)\sum_{i=1}^{2}\sum_{n=0}^{N-1}\varepsilon_{2i}(\rho_i + \Delta\rho_i\cos(\omega_o n - \phi_i))^2 dn\sin(\omega_o n - \varphi_o)\cos(\omega_o n - \varphi_o) \tag{34}$$

$$F_{d\varphi_o} = \cos^2(\theta)\sum_{i=1}^{2}\sum_{n=0}^{N-1}\varepsilon_{2i}(\rho_i + \Delta\rho_i\cos(\omega_o n - \phi_i))^2 d\sin(\omega_o n - \varphi_o)\cos(\omega_o n - \varphi_o) \tag{35}$$

$$\begin{aligned} F_{\omega_o\omega_o} &= \sum_{i=1}^{2}\sum_{n=0}^{N-1}\varepsilon_{1i}\Delta\rho_i^2 n^2\sin^2(\omega_o n - \phi_i) \\ &+ \cos^2(\theta)\sum_{i=1}^{2}\sum_{n=0}^{N-1}\varepsilon_{2i}(\rho_i + \Delta\rho_i\cos(\omega_o n - \phi_i))^2 d^2 n^2\sin^2(\omega_o n - \varphi_o) \end{aligned} \tag{36}$$

$$F_{\omega_o\varphi_o} = -\cos^2(\theta)\sum_{i=1}^{2}\sum_{n=0}^{N-1}\varepsilon_{2i}(\rho_i + \Delta\rho_i\cos(\omega_o n - \phi_i))^2 d^2 n\sin^2(\omega_o n - \varphi_o) \tag{37}$$

$$F_{\omega_o\Delta\rho_i} = -\sum_{n=0}^{N-1}\varepsilon_{1i}\Delta\rho_i n\sin(\omega_o n - \phi_i)\cos(\omega_o n - \phi_i),\ \ F_{\varphi_o\Delta\rho_i} = 0,\ F_{\varphi_o\phi_i} = 0 \tag{38}$$

$$F_{\omega_o\phi_i} = -\sum_{n=0}^{N-1}\varepsilon_{1i}\Delta\rho_i^2 n\sin^2(\omega_o n - \phi_i),\quad F_{\Delta\rho_i\phi_i} = \sum_{n=0}^{N-1}\varepsilon_{1i}\Delta\rho_i\cos(\omega_o n - \phi_i)\sin(\omega_o n - \phi_i) \tag{39}$$

$$F_{\varphi_o\varphi_o} = \cos^2(\theta)\sum_{i=1}^{2}\sum_{n=0}^{N-1}\varepsilon_{2i}(\rho_i + \Delta\rho_i\cos(\omega_o n - \phi_i))^2 d^2\sin^2(\omega_o n - \varphi_o) \tag{40}$$

$$F_{\Delta\rho_i\Delta\rho_i} = \sum_{n=0}^{N-1}\varepsilon_{1i}\cos^2(\omega_o n - \phi_i),\quad F_{\phi_i\phi_i} = \sum_{n=0}^{N-1}\varepsilon_{1i}\Delta\rho_i^2\sin^2(\omega_o n - \phi_i) \tag{41}$$

Since $h_i(n;\boldsymbol{\psi})$ depends only on ω_o and not on R_o, d, and φ_o, the FIM elements in (32) are zero. In fact the FIM elements for $\Delta\rho_i$ and ϕ_i depend on ω_o only and not on the rest of the parameters. The effect of $h_i(n;\boldsymbol{\psi})$ and hence $\Delta\rho_i$ is explained in the simulations section. Further simplifications of the FIM elements in eqs. (28-41) are shown in Appendix-B. For the special case of $h_i(n;\boldsymbol{\psi}) = 0, \Rightarrow \Delta\rho_i = 0, \forall i = 1,2$ corresponding to a vibrating target, the FIM is a function of the aspect angle θ, and the desired parameters are $\boldsymbol{\psi} = [R_o \quad d \quad \omega_o \quad \varphi_o]^T$. In order to simplify notation, the terms with θ are separated. We, therefore, obtain the final FIM as a Hadamard product of two matrices, the matrix $\mathbf{A}$ containing the terms in θ and the FIM, $\mathbf{F}$, corresponding to $\theta = 0$.

$$\mathbf{F}(\theta) = \mathbf{A} \circ \mathbf{F} = \begin{bmatrix} \mathbf{F_1} & \mathbf{F_3} \\ \mathbf{F_3}^T & \mathbf{F_2} \end{bmatrix} \tag{42}$$

where

$$\mathbf{A} = \begin{bmatrix} 1 & \cos(\theta) & \cos(\theta) & \cos(\theta) \\ \cos(\theta) & \cos^2(\theta) & \cos^2(\theta) & \cos^2(\theta) \\ \cos(\theta) & \cos^2(\theta) & \cos^2(\theta) & \cos^2(\theta) \\ \cos(\theta) & \cos^2(\theta) & \cos^2(\theta) & \cos^2(\theta) \end{bmatrix}, \quad \mathbf{F} = \begin{bmatrix} F_{R_o R_o} & F_{R_o d} & F_{R_o \omega_o} & F_{R_o \varphi_o} \\ F_{dR_o} & F_{dd} & F_{d\omega_o} & F_{d\varphi_o} \\ F_{\omega_o R_o} & F_{\omega_o d} & F_{\omega_o \omega_o} & F_{\omega_o \varphi_o} \\ F_{\varphi_o R_o} & F_{\varphi_o d} & F_{\varphi_o \omega_o} & F_{\varphi_o \varphi_o} \end{bmatrix} \tag{43}$$

Using numerical inversion it can be verified that $\mathbf{F}$ is positive definite (PD). However, from (43), $\mathbf{A}$ is rank one with one positive eigenvalue, $1+3\cos^2(\theta)$. Thus, $\mathbf{A}$ is positive semi-definite (PSD). Indeed, the Hadamard product of a PSD and a PD matrix is a cause for alarm, and prompts us to verify the non-singularity of $\mathbf{F}(\theta)$, without which the CRBs are unobtainable. Moreover, since $\mathbf{F}(\theta)$ represents a Fisher information matrix, it must at least be PSD, in which case the CRBs are infinite. The positive definiteness of $\mathbf{F}(\theta)$ can be proven using *Lemma-1,* implying non-singularity of the FIM [25]. In *Lemma-1*, the matrices are assumed complex, however the results can be generalized to real matrices. In [25], the authors have provided the complete definiteness characteristics of the Hadamard product of two matrices. However, in our case, it is sufficient to prove that $\mathbf{F}(\theta)$ is PD.

Lemma 1: Consider matrices $\mathbf{A}, \mathbf{B} \in C^{N \times N}$, where $\mathbf{A}$ is Hermitian PSD and $\mathbf{B}$ is Hermitian PD. Then, $\mathbf{A} \circ \mathbf{B}$ is PD if all the diagonal elements of $\mathbf{A}$ are not equal to zero.

Proof : This lemma is proved in [25, pg. 309, theorem 5.2.1]. The proof uses the Sylvester's law of inertia extensively.

The CRBs are present along the diagonal of $\mathbf{F}(\theta)^{-1}$. From *Lemma-1*, $\mathbf{F}(\theta)$ is invertible, we can simplify $\mathbf{F}(\theta)^{-1}$ as

$$\mathbf{F}(\theta)^{-1} = \begin{bmatrix} 1 & 1/\cos(\theta) & 1/\cos(\theta) & 1/\cos(\theta) \\ 1/\cos(\theta) & 1/\cos^2(\theta) & 1/\cos^2(\theta) & 1/\cos^2(\theta) \\ 1/\cos(\theta) & 1/\cos^2(\theta) & 1/\cos^2(\theta) & 1/\cos^2(\theta) \\ 1/\cos(\theta) & 1/\cos^2(\theta) & 1/\cos^2(\theta) & 1/\cos^2(\theta) \end{bmatrix} \circ \begin{bmatrix} F_{R_o R_o} & F_{R_o d} & F_{R_o \omega_o} & F_{R_o \varphi_o} \\ F_{dR_o} & F_{dd} & F_{d\omega_o} & F_{d\varphi_o} \\ F_{\omega_o R_o} & F_{\omega_o d} & F_{\omega_o \omega_o} & F_{\omega_o \varphi_o} \\ F_{\varphi_o R_o} & F_{\varphi_o d} & F_{\varphi_o \omega_o} & F_{\varphi_o \varphi_o} \end{bmatrix}^{-1} \tag{44}$$

For deriving (44), the theorem in Appendix-C was used. The inverse of the second matrix in (44) is tedious and, therefore, is computed using numerical techniques. It is evident from (44) that the parameter R_o is insensitive to θ, whereas the other parameters are sensitive to θ, depending on $\cos^2(\theta)$.

C. Accelerating target CRB

In this case, the parameter vector is defined by $\boldsymbol{\psi} = \begin{bmatrix} R_o & \alpha & \beta \end{bmatrix}^T$. The FIM can be derived from the general expression (21) using the range equation (16). Proceeding in the same fashion as before, i.e., using the Hadamard product approach, we obtain

$$\mathbf{F}(\theta) = \begin{bmatrix} 1 & \cos(\theta) & \cos(\theta) \\ \cos(\theta) & \cos^2(\theta) & \cos^2(\theta) \\ \cos(\theta) & \cos^2(\theta) & \cos^2(\theta) \end{bmatrix} \circ \begin{bmatrix} F_{R_oR_o} & F_{R_o\alpha} & F_{R_o\beta} \\ F_{\alpha R_o} & F_{\alpha\alpha} & F_{\alpha\beta} \\ F_{\beta R_o} & F_{\beta\alpha} & F_{\beta\beta} \end{bmatrix} \tag{45}$$

where

$$F_{R_oR_o} = \sum_{i=1}^{2} \rho_i^2 \varepsilon_{2i} N,\ F_{R_o\alpha} = \sum_{i=1}^{2} \sum_{n=0}^{N-1} \rho_i^2 \varepsilon_{2i} n = \frac{N(N-1)}{2} \sum_{i=1}^{2} \rho_i^2 \varepsilon_{2i} \tag{46a}$$

$$F_{R_o\beta} = \sum_{i=1}^{2} \sum_{n=0}^{N-1} \rho_i^2 \varepsilon_{2i} n^2 = \frac{N(N-1)(2N-1)}{6} \sum_{i=1}^{2} \rho_i^2 \varepsilon_{2i} \tag{46b}$$

$$F_{\alpha\alpha} = \sum_{i=1}^{2} \sum_{n=0}^{N-1} \rho_i^2 \varepsilon_{2i} n^2 = \frac{N(N-1)(2N-1)}{6} \sum_{i=1}^{2} \rho_i^2 \varepsilon_{2i} \tag{47a}$$

$$F_{\alpha\beta} = \sum_{i=1}^{2} \sum_{n=0}^{N-1} \rho_i^2 \varepsilon_{2i} n^3 = \frac{N^2(N-1)^2}{4} \sum_{i=1}^{2} \rho_i^2 \varepsilon_{2i} \tag{47b}$$

$$F_{\beta\beta} = \sum_{i=1}^{2} \sum_{n=0}^{N-1} \rho_i^2 \varepsilon_{2i} n^4 = \left(\frac{N^5}{5} - \frac{N^4}{2} + \frac{N^3}{3} - \frac{N}{30} \right) \sum_{i=1}^{2} \rho_i^2 \varepsilon_{2i} \tag{48}$$

The CRB's after inverting the FIM, are given by

$$CRB(R_o) = \frac{3}{(\rho_1^2 \varepsilon_{21} + \rho_2^2 \varepsilon_{22})} \times \frac{3N^2 - 3N + 2}{N(N^2 + 3N + 2)} \tag{49}$$

$$CRB(\alpha) = \frac{12}{\cos^2(\theta)(\rho_1^2 \varepsilon_{21} + \rho_2^2 \varepsilon_{22})} \times \frac{16N^2 - 30N + 11}{N(N^4 - 5N^2 + 4)} \tag{50}$$

$$CRB(\beta) = \frac{1}{\cos^2(\theta)(\rho_1^2\varepsilon_{21} + \rho_2^2\varepsilon_{22})} \times \frac{180}{N(N^4 - 5N^2 + 4)} \tag{51}$$

where ε_{2i} is defined before and includes both carrier frequency and noise variance terms.

IV. Simulation and Quasi-Experimental Results

A. Numerical Simulations

We begin by examining the effect of θ on the CRBs. The term $1/\cos^2(\theta)$ in the CRBs will simply increase the CRBs for increased value of θ. The CRB's become infinite when $\theta = \pm\pi/2$. Moreover, $\theta = \pm\pi/2$ yields a singular FIM. The minimum CRB is achieved when $\theta = 0$, i.e., when the target is moving along the LOS of the radar system. Without loss of generality, in the simulations we assume, $\rho_i = \rho$, and $h_i(n;\boldsymbol{\psi}) = h(n;\boldsymbol{\psi}), \forall i = 1,2$. This then implies $\Delta\rho_i = \Delta\rho$ and $\phi_i = \phi$. The SNR for constant Doppler and accelerating target motion profiles, are denoted by $SNR_i = \rho^2/\sigma_i^2$, $i = 1,2$ for the two carriers respectively. Fig 1 illustrates the sensitivity of the CRBs for the constant Doppler and accelerating target motion profiles, the carrier frequencies were chosen to be $f_1 = 906$ MHz and $f_2 = 919$ MHz. Fig. 2 shows the CRBs for the MD motion profile for the vibration model ($\Delta\rho = 0$), and the rotation model. We define SNR for MD as $SNR_i = (\rho + \Delta\rho)^2/\sigma_i^2$, $i = 1,2$. In order to be fair in our comparison, the SNR for both the vibration and rotation models was assumed identical in Fig. 2, and the parameters for vibration and rotation model are subscripted by '*v*' and '*r*' respectively. Fig. 2 clearly shows that the CRBs for the rotation model are higher than those of the vibration model for the same SNRs. It is well known that the CRBs of the phase parameters increase with the bandwidth of the signal amplitude [22, 26]. The bandwidth of the amplitude for the vibration model is zero (DC), whereas, bandwidth of the amplitude for the rotation model is ω_o. Indeed, the scalar function $h(n;\boldsymbol{\psi})$ in the rotation model smears the exponential part of the returns and makes parameter estimation more difficult. In Fig. 1 we observe that v has higher sensitivity than R_o, since it has a lower CRB for increasing N

[22]. Similarly, from Fig. 1, the chirp, or the accelerating target parameter β, is the most sensitive, whereas R_o is the least sensitive. From Fig. 2, for data record length $N > 50$, the parameter ω_o is the most sensitive. It is noteworthy that the CRB for R_o is much lower than the CRB for parameter d, both of which have the same units of measurement and represent a distance and displacement, respectively. Sensitivity of the parameters, as evidenced by the CRBs, are an indication of some order of estimation of the parameters. For example, we have seen that v is the most sensitive parameter for the constant Doppler motion and it represents the frequency in the sinusoidal parameter estimation problem, whereas R_o represents the phase in the sinusoidal parameter estimation model. It is well known that the maximum likelihood estimator (MLE) for the sinusoidal parameter model estimates the frequency first, and then the phase [15]. Similarly, for the PPS signal model, the highest order PPS coefficient is estimated first, and the lower orders are estimated subsequently [23, 26-28]. In our case, this agrees with β being the most sensitive for a second order PPS signal, i.e. the accelerating target returns. For the case of MD, we have a suboptimal estimator already in place in eqs. (13-14). Clearly, taking the Fourier transform of the MD returns, using the DC as a reference, and selecting the two nearest peaks around 0 Hz is the quickest way to estimate ω_o.

B. Quasi-Experimental results

In urban sensing applications, the rotational or the vibrational frequency is an important parameter for differentiating animate from inanimate targets. An indoor rotating fan with three plastic blades was used as the target for the real-data collection experiment. In order to obtain strong single component returns, one of the blades was wrapped in aluminum foil. The carrier frequencies of the dual-frequency radar were chosen to be $f_1 = 906.3$ MHz, and $f_2 = 919.8$ MHz, and the sampling frequency was set to 1 kHz. The radar returns at the two frequencies were simultaneously collected for a total duration of 1s. The center of rotation of the fan was at a distance of 1.22m from the antenna feed point along the LOS. The rotation speed of the fan was measured to be 780 rpm, which is in agreement with the technical specifications of the fan, and is considered to be the true value of the parameter ω_o. The objective is to estimate the

rotational frequency of the fan for varying SNRs, and compute its variance for comparison with the CRB. The data is at a high SNR and is virtually noise free. In order to vary the SNR, we add complex white Gaussian noise. Hence the term quasi-experimental is used. Since no estimation technique has been advocated in this paper, we use the Fourier domain analysis, as given by eqs. (13-14) and extract the frequency of the first harmonic. This procedure is definitely suboptimal, the optimal method of maximum likelihood is not pursued here due to its associated computational complexity [24]. Extracting the first harmonic frequency is sufficient to obtain the estimate of the rotational frequency, since typically indoor inanimate targets are NBFM, see [24] for more details on estimating harmonics of NBFM. The FIM for MD is a function of the parameters d and φ_o, which are unknown. Furthermore, the amplitudes of the returns are also unknown. We employ some suboptimal schemes to estimate these and use these in our FIM calculations. The estimation of the unknown parameters is performed using the real data without adding artificial noise, these estimates are then considered as the true parameters. In particular, since the amplitudes of the returns are unknown, and, in general, are time-varying, the amplitudes can be efficiently estimated using the second order cyclic moment, see [28] and references therein. On the other hand, the time-frequency (TF) distribution is particularly useful in extracting the parameter d. The maximum and minimum instantaneous frequencies of the MD signal are given by $\pm 2 f_i d \omega_o / c$ corresponding to the two carrier frequencies, respectively. The bandwidth of the MD signal can then be defined as $4 f_i d \omega_o / c$. The bandwidth is estimated from the original returns using the spectrogram, and since the rotational frequency is known, computation of d is straightforward, this value is then taken as the true parameter value. The return for the first carrier was used for calculating d. For estimating the phase φ_o, we use the least squares estimator as in [24], with $K = 1$ using the returns corresponding to the first carrier frequency. For this procedure, the returns were zero padded and an 8192 point FFT was computed. These parameters were then used in computing the CRBs. Fig. 3(a) shows the spectrogram of the original returns corresponding to the carrier f_1. It also shows the signature using the estimated d and φ_o, and the true rotational frequency ω_o as a solid black line, which closely follows the TF signature of the returns. The

maximum and minimum of instantaneous frequency are depicted with the dotted black lines. In Fig. 3(b), the raw FFT of the returns corresponding to the carrier f_1 is shown, Fig. 3(c) shows the estimated second order cyclic moment for the carrier frequency f_1, and Fig. 3(d) shows the real part of the returns for the first carrier. From Fig. 3(c) it is clear that the second order cyclic moment shows harmonics at the rotational frequency ω_o, indicating the cyclic RCS changes, and hence validating the cyclic amplitude modulation we have assumed for the MD rotational model. We are now in a position to compute the CRB and the simulated mean square error (MSE) using Monte Carlo simulations. Fig. 4 shows the CRB for the rotational frequency and the MSE of its estimates vs. SNRs, 100 Monte Carlo trials was used in the simulations. For each carrier frequency, the initial estimate was derived from a raw FFT search, and subsequently the chirp-z transform was used to compute the final estimate of the first harmonic around the coarse initial estimate from the FFT, the search span of the chirp-z transform was 8192 points. This estimation procedure is identical to that used in [24] with $K = 1$. The final estimate of the rotational frequency was the average of these estimates for the two carrier frequencies. A strong and consistent bias of the order 10^{-3} was observed in the raw MSE for SNR $\geq$ 20 dB, as shown in Fig. 4, the bias-corrected MSE is also shown and comes close to the CRB for the rotational model. The strong bias maybe due to the chirp-z transform, necessitating optimization methods to be employed for estimation, for example the non-linear least squares. For comparison, the CRB for the vibration model (the single frequency and dual frequency) are also shown, the simulated MSE is far away from the vibration model CRBs.

V. Conclusions

In this paper, we considered dual frequency radar for range estimation with application to urban sensing. Three important and commonly encountered indoor range profiles were considered, namely, linear translation, micro-Doppler and accelerating target motion profiles. The CRBs were derived for the initial range and key target classification parameters, namely, velocity, acceleration and oscillatory frequency of targets respectively, encountering linear, accelerating, and simple harmonic motions. A parametric model specific to the dual frequency radar technique was developed for the range profiles, incorporating the

target aspect angles. It was shown that if the aspect angle is unknown, then the FIM becomes singular, leading to unidentifiability of the parameters. Closed form expressions for CRBs were derived for the parameters associated with translational motion profiles. However, for the MD case, the CRBs were intractable in closed form, and numerical matrix inversion was pursued. It was also shown that the dual-frequency approach provides lower bounds as compared to the single frequency counterpart.

APPENDIX-A

We demonstrate by example, when θ is unknown and is a desired parameter, the FIM is singular. Specifically, the derivation is for the constant Doppler range profile, the derivation can be generalized to any other motion profile. For convenience, and without loss of generality, we assume $\rho_i = \rho$. The parameter vector sought after is $\boldsymbol{\psi} = [R_o \quad v \quad \theta]$. Using (17) and (9), and skipping the trivial details

$$\mathbf{F}(\theta) = \begin{bmatrix} F_{R_oR_o} & F_{R_ov} & F_{R_o\theta} \\ F_{R_ov} & F_{vv} & F_{v\theta} \\ F_{R_o\theta} & F_{v\theta} & F_{\theta\theta} \end{bmatrix}$$

$$\begin{bmatrix} \varepsilon N & \dfrac{\varepsilon\cos(\theta)N(N-1)}{2} & \dfrac{-v\varepsilon\sin(\theta)N(N-1)}{2} \\ \dfrac{\varepsilon\cos(\theta)N(N-1)}{2} & \dfrac{\varepsilon\cos^2(\theta)N(N-1)(2N-1)}{6} & \dfrac{-v\varepsilon\sin(2\theta)N(N-1)(2N-1)}{12} \\ \dfrac{-v\varepsilon\sin(\theta)N(N-1)}{2} & \dfrac{-v\varepsilon\sin(2\theta)N(N-1)(2N-1)}{12} & \dfrac{\varepsilon v^2\sin^2(\theta)N(N-1)(2N-1)}{6} \end{bmatrix} \quad \text{(A.1)}$$

It can be shown that the FIM is singular, implying non-identifiable parameters for the chosen model [29]. This can, however, be overcome if an additional carrier diverse radar system, oriented differently from the original radar system, is used. This involves an additional angle diversity term in the Fisher information. Moreover, the orientation of the two radars with respect to each other must be known for identifiability.

APPENDIX-B

In order to bring the FIM elements for MD in closed form, we need the following which can be derived easily using elementary trigonometry, and elementary calculus. The series are assumed to uniformly converge so that the differential and summation operators can be interchanged.

$$g_1(\omega,\psi)=\sum_{n=0}^{N-1}\cos(\omega n-\psi)=\mathrm{Re}\left\{\sum_{n=0}^{N-1}e^{j(\omega n-\psi)}\right\}=\frac{\cos(\omega(N-1)/2-\psi)\sin(\omega N/2)}{\sin(\omega/2)} \tag{B.1}$$

$$g_2(\omega,\psi)=\sum_{n=0}^{N-1}\sin(\omega n-\psi)=\mathrm{Im}\left\{\sum_{n=0}^{N-1}e^{j(\omega n-\psi)}\right\}=\frac{\sin(\omega(N-1)/2-\psi)\sin(\omega N/2)}{\sin(\omega/2)} \tag{B.2}$$

$$g_3(\omega,\psi)=\sum_{n=0}^{N-1}-n\sin(\omega n-\psi)=\frac{\partial g_1(\varpi,\psi)}{\partial\omega}=\frac{1}{4\sin^2\left(\frac{\omega}{2}\right)}\begin{pmatrix}(2N-1)\sin\frac{\omega}{2}\cos\left(\omega\frac{2N-1}{2}-\psi\right)\\-\cos\frac{\omega}{2}\sin\left(\omega\frac{2N-1}{2}-\psi\right)-\sin(\psi)\end{pmatrix} \tag{B.3}$$

$$\begin{aligned}g_4(\omega,\psi)&=\sum_{n=0}^{N-1}n^2\sin^2(\omega n-\psi)=\frac{1}{2}\sum_{n=0}^{N-1}(n^2-n^2\cos(2\omega n-2\psi))\\&=\frac{1}{2}\left(\frac{N(N-1)(2N-1)}{6}+\frac{\partial g_3(\omega,\psi)}{\partial\omega}|_{\omega=2\omega,\psi=2\psi}\right)\\&=\frac{1}{2}\left(\frac{N(N-1)(2N-1)}{6}+\frac{1}{8\sin^3(\omega)}\begin{pmatrix}2\cos^2(\omega)\sin(\omega(2N-1)-2\psi)\\+2\cos(\omega)\sin(2\psi)\\-\begin{pmatrix}(2N-1)\sin(2\omega)\\\times\cos(\omega(2N-1)-2\psi)\end{pmatrix}\\-\begin{pmatrix}4N(N-1)\sin^2(\omega)\\\times\sin(\omega(2N-1)-2\psi)\end{pmatrix}\end{pmatrix}\right)\end{aligned} \tag{B.5}$$

$$g_5(\omega,\psi)=\sum_{n=0}^{N-1}n^2\cos^2(\omega n-\psi)=\frac{N(N-1)(2N-1)}{6}-g_4(\omega,\psi) \tag{B.7}$$

$$g_6(\omega,\psi)=\sum_{n=0}^{N-1}n^2\cos(\omega n-\psi)=\frac{-\partial g_3(\omega,\psi)}{\partial\omega}=\frac{N(N-1)(2N-1)}{6}-2g_4(\omega/2,\psi/2) \tag{B.8}$$

$$\begin{aligned}g_7(\omega,\psi)&=\sum_{n=0}^{N-1}-n\cos(\omega n-\psi)=-\frac{\partial g_2(\omega n-\psi)}{\partial\omega}\\&=\frac{-1}{4\sin^2(\omega/2)}\begin{pmatrix}(2N-1)\sin\frac{\omega}{2}\sin\left(\omega\frac{2N-1}{2}-\psi\right)\\+\cos\frac{\omega}{2}\cos\left(\omega\frac{2N-1}{2}-\psi\right)-\cos(\psi)\end{pmatrix}\end{aligned} \tag{B.10}$$

$$g_8(\omega,\psi)=\sum_{n=0}^{N-1}-n\sin^2(\omega n-\psi)=\frac{1}{2}\left(-N(N-1)/2-g_7(2\omega,2\psi)\right) \tag{B.11}$$

We are now in a position to express the FIM elements in closed form. The following can be readily shown

$$F_{R_o R_o} = \sum_{i=1}^{2} \varepsilon_{2i} \left(\rho_i^2 N + 2\rho_i \Delta\rho_i g_1(\omega_o, \phi_i) + \frac{\Delta\rho_i^2 (g_1(2\omega_o, 2\phi_i) + N)}{2} \right) \tag{B.12}$$

$$F_{R_o d} = \cos(\theta) \sum_{i=1}^{2} \varepsilon_{2i} \left(\begin{array}{c} (\rho_i^2 + \Delta\rho_i^2 / 2) g_1(\omega_o, \varphi_o) + \frac{\Delta\rho_i^2 (g_1(3\omega_o, \varphi_o + 2\phi_i) + g_1(\omega_o, 2\phi_i - \varphi_o)}{4} \\ + \rho_i \Delta\rho_i (g_1(2\omega_o, \varphi_o + \phi_i) + N\cos(\varphi_o - \phi_i) \end{array} \right) \tag{B.13}$$

$$F_{R_o \omega_o} = \cos(\theta) \sum_{i=1}^{2} \varepsilon_{2i} \left(\begin{array}{c} (\rho_i^2 d + \Delta\rho_i^2 d / 2) g_3(\omega_o, \varphi_o) + \rho_i \Delta\rho_i d g_3(2\omega_o, \varphi_o + \phi_i) \\ -\rho_i \Delta\rho_i d \sin(\phi_i - \varphi_o) N(N-1)/2 + \Delta\rho_i^2 d g_3(3\omega_o, \varphi_o + 2\phi_i)/4 \\ -\Delta\rho_i^2 d g_3(\omega_o, \varphi_o - 2\phi_i)/4 \end{array} \right) \tag{B.14}$$

$$F_{R_o \varphi_o} = \cos(\theta) \sum_{i=1}^{2} \varepsilon_{2i} \left(\begin{array}{l} (\rho_i^2 d + \Delta\rho_i^2 d / 2) g_2(\omega_o, \varphi_o) + \rho_i \Delta\rho_i d g_2(2\omega_o, \varphi_o + \phi_i) - \rho_i \Delta\rho_i d \sin(\phi_i - \varphi_o) N \\ + \Delta\rho_i^2 d g_2(3\omega_o, \varphi_o + 2\phi_i)/4 - \Delta\rho_i^2 d g_2(\omega_o, \varphi_o - 2\phi_i)/4 \end{array} \right) \tag{B.15}$$

$$F_{R_o \Delta\rho_i} = 0,\ F_{R_o \phi_i} = 0,\ \ F_{d\Delta\rho_i} = 0,\ F_{d\phi_i} = 0 \tag{B.16}$$

$$F_{dd} = \cos^2(\theta) \sum_{i=1}^{2} \varepsilon_{2i} \left(\begin{array}{l} \rho_i^2 (N + g_1(2\omega_o, 2\varphi_o))/2 + \rho_i \Delta\rho_i g_1(\omega_o, \phi_i) + \rho_i \Delta\rho_i g_1(3\omega_o, 2\varphi_o + \phi_i)/2 \\ + \rho_i \Delta\rho_i g_1(\omega_o, 2\varphi_o - \phi_i)/2 + \Delta\rho_i^2 (N + g_1(2\omega_o, 2\phi_i) + g_1(2\omega_o, 2\varphi_o))/4 \\ + \Delta\rho_i^2 (N + g_1(4\omega_o, 2\phi_i + 2\varphi_o) + N\cos(2\varphi_o - 2\phi_i))/8 \end{array} \right) \tag{B.17}$$

$$F_{d\omega_o} = \cos^2(\theta) \sum_{i=1}^{2} \varepsilon_{2i} \left(\begin{array}{l} \rho_i^2 d g_3(2\omega_o, 2\varphi_o)/2 + \rho_i \Delta\rho_i d g_3(3\omega_o, 2\varphi_o + \phi_i)/2 + \rho_i \Delta\rho_i d g_3(\omega_o, 2\varphi_o - \phi_i)/2 \\ + \Delta\rho_i^2 d (g_3(4\omega_o, 2\varphi_o + 2\phi_i) - N(N-1)\sin(2\phi_i - 2\varphi_o)/2)/8 + \Delta\rho_i^2 d g_3(2\omega_o, 2\varphi_o)/4 \end{array} \right) \tag{B.18}$$

$$F_{d\varphi_o} = \cos^2(\theta) \sum_{i=1}^{2} \varepsilon_{2i} \left(\begin{array}{l} \rho_i^2 d g_2(2\omega_o, 2\varphi_o)/2 + \rho_i \Delta\rho_i d g_2(3\omega_o, 2\varphi_o + \phi_i)/2 + \rho_i \Delta\rho_i d g_2(\omega_o, 2\varphi_o - \phi_i)/2 \\ + \Delta\rho_i^2 d (g_2(4\omega_o, 2\varphi_o + 2\phi_i) + N\sin(2\phi_i - 2\varphi_o))/8 + \Delta\rho_i^2 d g_2(2\omega_o, 2\varphi_o)/4 \end{array} \right) \tag{B.19}$$

$$\begin{aligned} F_{\omega_o \omega_o} &= \sum_{i=1}^{2} \varepsilon_{1i} \Delta\rho_i^2 g_4(\omega_o, \phi_i) \\ &+ \cos^2(\theta) \sum_{i=1}^{2} \varepsilon_{2i} \left(\begin{array}{l} \rho_i^2 d^2 g_4(\omega_o, \varphi_o) + \rho_i \Delta\rho_i g_5(\omega_o, \phi_i) \\ -\rho_i \Delta\rho_i d^2 (g_6(3\omega_o, \phi_i + 2\varphi_o) + g_6(\omega_o, 2\varphi_o - \phi_i))/2 \\ + \Delta\rho_i^2 d^2 (N(N-1)(2N-1)/6)/4 \\ -\Delta\rho_i^2 d^2 (g_6(2\omega_o, 2\phi_i) - g_6(2\omega_o, 2\varphi_o))/4 \\ -\Delta\rho_i^2 d^2 (g_6(4\omega_o, 2\phi_i + 2\varphi_o) + N(N-1)(2N-1)\cos(2\phi_i - 2\varphi_o)/6)/8 \end{array} \right) \end{aligned} \tag{B.20}$$

$$F_{\omega_o\varphi_o} = \cos^2(\theta)\sum_{i=1}^{2}\varepsilon_{2i}\begin{pmatrix} \rho_i^2 d^2 g_8(\omega_o,\varphi_o) + \rho_i\Delta\rho_i d^2 g_7(\omega_o,\phi_i) \\ -\rho_i\Delta\rho_i d^2(g_7(3\omega_o,\phi_i+2\varphi_o)+g_7(\omega_o,2\varphi_o-\phi_i))/2 \\ -\Delta\rho_i^2 d^2 N(N-1)/8 \\ +\Delta\rho_i^2 d^2(g_7(2\omega_o,2\phi_i)-g_7(2\omega_o,2\varphi_o))/4 \\ +\Delta\rho_i^2 d^2(N(N-1)\cos(2\phi_i-2\varphi_o)/2-g_7(4\omega_o,2\phi_i+2\varphi_o))/8 \end{pmatrix} \tag{B.21}$$

$$F_{\omega_o\Delta\rho_i} = \varepsilon_{1i}\Delta\rho_i g_3(2\omega_o,2\phi_i)/2,\;\; F_{\omega_o\phi_i} = \varepsilon_{1i}\Delta\rho_i^2(-g_7(2\omega_o,2\phi_i)-N)/2 \tag{B.22}$$

$$F_{\varphi_o\varphi_o} = \cos^2(\theta)\sum_{i=1}^{2}\varepsilon_{2i}\begin{pmatrix} \rho_i^2 d^2(N-g_1(2\omega_o,2\varphi_o))/2+\rho_i\Delta\rho_i d^2 g_1(\omega_o,\phi_i) \\ -\rho_i\Delta\rho_i d^2(g_1(3\omega_o,2\varphi_o+\phi_i)+g_1(\omega_o,2\varphi_o-\phi_i))/2 \\ +\Delta\rho_i^2 d^2(N-g_1(2\omega_o,2\varphi_o)+g_1(2\omega_o,2\phi_i))/4 \\ -\Delta\rho_i^2 d^2(N\cos(2\varphi_o-2\phi_i)+g_1(4\omega_o,2\varphi_o+2\phi_i))/8 \end{pmatrix} \tag{B.23}$$

$$F_{\varphi_o\Delta\rho_i} = 0,\; F_{\varphi_o\phi_i} = 0,\;\; F_{\Delta\rho_i\Delta\rho_i} = \varepsilon_{1i}(N+g_1(2\omega_o,2\phi_i))/2 \tag{B.24}$$

$$F_{\Delta\rho_i\phi_i} = \varepsilon_{1i}\Delta\rho_i g_2(2\omega_o,2\phi_i)/2,\;\; F_{\phi\phi} = \varepsilon_{1i}\Delta\rho_i(N-g_1(2\omega_o,2\phi_i))/2 \tag{B.25}$$

APPENDIX-C

Theorem-1: Let $\mathbf{A}$, $\mathbf{B}$ be two complex matrices $\in C^{N\times N}$. The rank of $\mathbf{A}$ is one with non-zero diagonal elements and the rank of $\mathbf{B}$ is N. Then $(\mathbf{A}\circ\mathbf{B})^{-1} = \mathbf{B}^{-1}\circ(\mathbf{A}^{\circ-1})^T = \mathbf{B}^{-1}\circ(\mathbf{A}^T)^{\circ-1}$, where $\mathbf{A}^{\circ-1} = [a_{ij}^{-1}]$.

Proof: Since $\mathbf{A}$ is rank one, it can be rewritten as an outer product, given by

$$\mathbf{A} = \mathbf{x}\mathbf{y}^H,\; \mathbf{A}^T = \mathbf{y}^*\mathbf{x}^T,\; \text{with } \mathbf{x},\; \mathbf{y}\in C^{N\times 1} \tag{C.1}$$

The Hadamard product can then be expressed as

$$\mathbf{A}\circ\mathbf{B} = \mathbf{B}\circ\mathbf{x}\mathbf{y}^H = \mathbf{D}_{\mathbf{x}}\mathbf{B}\mathbf{D}_{\mathbf{y}}^H \tag{C.2}$$

where

$$\mathbf{D}_{\mathbf{x}} = Diag[\mathbf{x}] = \begin{bmatrix} x_1 & & \\ & \ddots & \\ & & x_N \end{bmatrix},\; \mathbf{D}_{\mathbf{y}} = Diag[\mathbf{y}] = \begin{bmatrix} y_1 & & \\ & \ddots & \\ & & y_N \end{bmatrix} \tag{C.3}$$

It is also clear from (C.2) that $\mathbf{A}\circ\mathbf{B}$ is non-singular. At this stage it is instructive to note that if any diagonal element of $\mathbf{A}$ is zero, which is tantamount to any element in (C.3) being zero, then the inverse

of $\mathbf{A} \circ \mathbf{B}$ does not exist. This is primarily the reason for imposing the condition, that none of the diagonal elements of $\mathbf{A}$ are zero in the statement of the theorem. The proof is straightforward from hereon, from (C.2)

$$(\mathbf{A} \circ \mathbf{B})^{-1} = (\mathbf{D}_{\mathbf{y}}^{H})^{-1} \mathbf{B}^{-1} \mathbf{D}_{\mathbf{x}}^{-1} \tag{C. 4}$$

Rewriting the diagonal matrices in terms of the Hadamard and the outer products as in (C.2), we get

$$(\mathbf{A} \circ \mathbf{B})^{-1} = \mathbf{B}^{-1} \circ \begin{bmatrix} 1/y_1^* \\ . \\ . \\ . \\ 1/y_N^* \end{bmatrix} \begin{bmatrix} 1/x_1 & . & . & . & 1/x_N \end{bmatrix} = \mathbf{B}^{-1} \circ (\mathbf{y}^{\circ -1})^* (\mathbf{x}^{\circ -1})^T \tag{C.5}$$

Expanding the outer product and rewriting the elements in terms of $\mathbf{A}$, we obtain

$$(\mathbf{A} \circ \mathbf{B})^{-1} = \mathbf{B}^{-1} \circ (\mathbf{A}^{\circ -1})^T = \mathbf{B}^{-1} \circ (\mathbf{A}^T)^{\circ -1} \tag{C. 6}$$

It must be noted that if $\mathbf{A}$ has a rank greater than one, then the inverse of the Hadamard product is quite complicated to derive. Fortunately, such a situation does not arise in this paper.

Acknowledgment

This work was supported in part by DARPA under contract HR0011-07-1-0001 and in part by ONR under grant N00014-07-1-0043. The content of the information does not necessarily reflect the position or policy of the government, and no official endorsement should be inferred. Approved for public release.

References

[1] Journal of the Franklin Institute, Special Issue on 'Advances in Indoor Radar Imaging,' Sept. 2008, 345, (6)

[2] Proceedings of the 2008 IEEE International Conference on Acoustics, Speech, and Signal Processing, Special Session on 'Through-the-Wall Radar Imaging,' Las vegas, USA, April 2008, pp. 5173-5196

[3] Borek, S. E.: 'An overview of through the wall surveillance for homeland security', Proc. 34th Applied Imagery and Pattern Recognition Workshop, Washington D.C., USA, Oct. 2005

[4] Proceedings of the 2005 IEEE AP-S International Symposium, Special Session on 'Through-Wall Imaging and Sensing', Washington D.C., USA, July 2005, 3B, pp. 317-341

[5] Skolnik , M. I.: 'Introduction to Radar Systems' (McGraw-Hill, New York, 3 rd edn. 2002)

[6] Ridenour, L. N.: 'Radar System Engineering', Vol. 1 of MIT Radiation Labaratory Series (McGraw-Hill, NY, 1947)

[7] Amin, M., Zemany, Setlur, P., and Ahmad, F.: 'Moving target localization for indoor imaging using dual frequency CW radars', Proc. IEEE Workshop on Sensor Array and Multi-channel Processing, Waltham, Massachusetts, USA, Jul. 12-14, 2006, pp. 367-371

[8] Boyer, W. D.: 'A diplex, Doppler, phase comparison radar', IEEE Trans. Aerosp. Navig. Electron., 1963, ANE-10, (3), pp. 27-33

[9] Dingley, G., and Alabaster, C.: 'Radar based automatic target system', Proc. Fourth Int. Waveform Diversity and Design Conf., Orlando, FL, USA, Feb. 2009, pp. 22-25

[10] Setlur, P., Amin, M., and Ahmad, F.: 'Cramer-Rao bounds for range and motion parameter estimations using dual frequency radars', Proc. Int. Conf. Acoust., Speech Signal Process., Honolulu, Hawaii, Apr. 15-20, 2007

[11] Haykin, S.: 'Communication Systems' (John Wiley, New York, 4 th edn. May 2000)

[12] Ahmad, F., Amin, M. G., and Zemany, P. D.: 'Performance analysis of dual-frequency CW radars for motion detection and ranging in urban sensing applications', Proc. SPIE Defense and Security Symposium, Orlando FL, USA, April 2007

[13] Ahmad, F., Amin, M. G., and Zemany, P. D.: 'Dual-frequency radars for target localization in urban sensing', IEEE Trans. on Aerospace and Electronic Systems, In Press.

[14] Zhang, Y., Amin, M. G., and Ahmad F.: 'Time-frequency analysis for the localization of multiple moving targets using dual-frequency radars', IEEE Signal Processing Letters, 2008, 15, pp. 777-780

[15] Kay, S. M.: 'Modern Spectral Estimation: Theory and Application' (Prentice Hall, Englewood Cliffs, NJ, 1988)

[16] Rife, D., and Boorstyn, R.: 'Single tone parameter estimation from discrete-time observations', IEEE Trans. Inf. Theory, Sep. 1974, 20, (5), pp. 581-598

[17] Chen, V. C., Li, F., Ho, S. –S., and Wechsler, H.: 'Micro-Doppler effect in radar: phenomenon, model, and simulation study', IEEE Trans. Aerosp. Electron. Syst., January 2006, 42, (1), pp. 2-21

[18] Abromowitz, M. and Stegun, I. A.: 'Handbook of Mathematical Functions with Formulas, Graphs, and Mathematical tables' (Dover Publications, New York, 1972)

[19] Grewal, B. S.: 'Higher Engineering Mathematics', (Khanna Publishers, New Delhi, India, 2002)

[20] Peleg, S., and Porat, B.: 'The Cramér-Rao lower bound for signals with constant amplitude and polynomial phase', IEEE Trans. Signal Process., Mar. 1991, 39, (3), pp. 749-752

[21] Zoubir, A. M. and Taleb, A.: 'The Cramer-Rao bound for the estimation of noisy phase signals', Proc. Int. Conf. Acoust. , Speech Signal Process., Salt Lake City, Utah, USA, May 2001

[22] Kay, S. M.: 'Fundamentals of Statistical Signal Processing, Volume: I, Estimation Theory' (Prentice Hall, Englewood Cliffs, NJ, 1993)

[23] Cirillo, L., Zoubir, A., and Amin, M.: 'Parameter estimation for locally linear FM signals using a time-frequency Hough transfrom', IEEE Trans. Signal Process., September 2008, 56, (9), pp. 4162-4175

[24] Gini, F., and Giannakis, G. B.: 'Hybrid FM-polynomial phase signal modeling: parameter estimation and Cramér-Rao bounds', IEEE Trans. Signal Process., February 1999, 47, (2), pp. 363-377

[25] Horn, R. A., and Johnson, C. R.:, 'Topics in Matrix Analysis' (Cambridge University Press, Cambridge, UK, 1991)

[26] Ghogho, M., Swami, A., and Nandi, A. K.: 'Cramér-Rao bounds and maximum likelihood estimation for random amplitude phase modulated signals', IEEE Trans. Signal Process., Nov. 1999, 47, (11), pp. 2905-2916

[27] Barbarossa, S., Scaglione, A., and Giannakis, G. B.: 'Product high-order ambiguity function for multicomponent polynomial-phase signal modeling', IEEE Trans. Signal Process., March 1998, 46, (3), pp. 691-708

[28] Ghogho, M., Swami, A., and Garel, B.: 'Performance analysis of cyclic statistics for the estimation of harmonics in multiplicative and additive noise', IEEE Trans. Signal Process., December 1999, 47, (12), pp. 3235-3249

[29] Stoica, P., and Marzetta, T. L.: 'Parameter estimation problems with singular information matrices', IEEE Trans. Signal Process., Jan. 2001, 49, (1), pp. 87-90

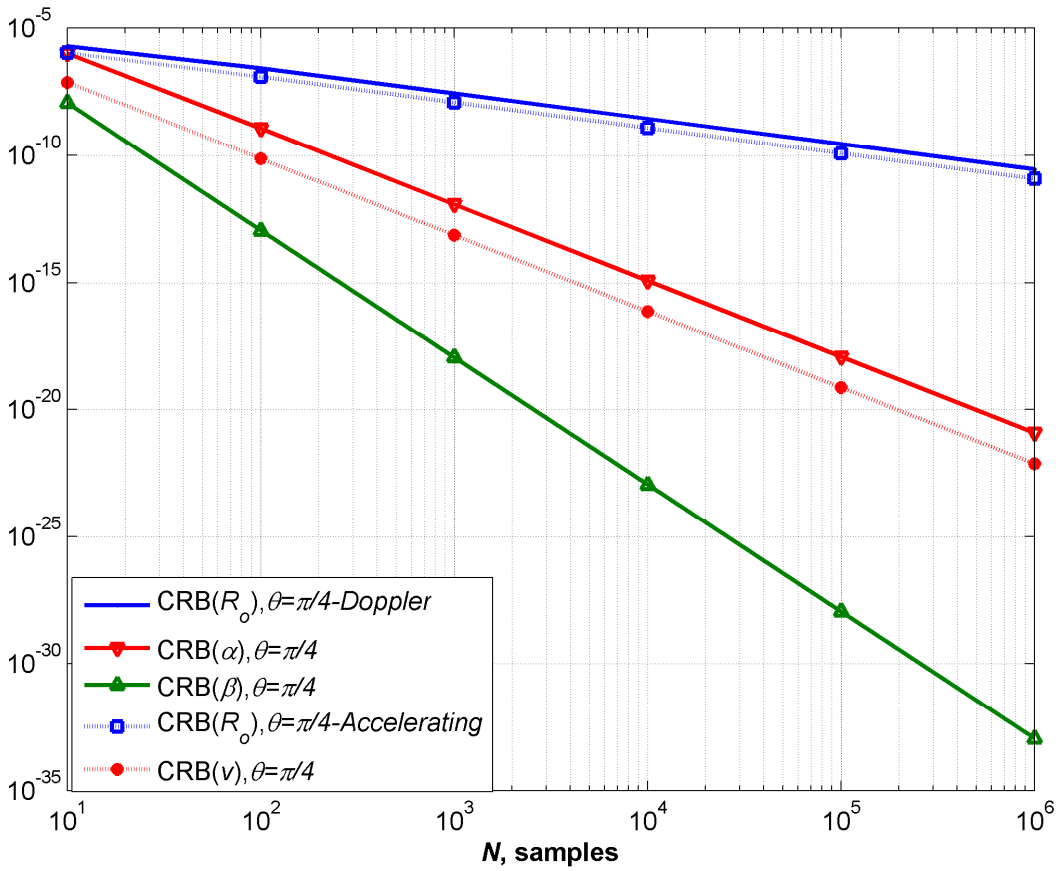

Fig.1. Constant Doppler and accelerating target CRB's for $(SNR1,\ SNR2) = (10, 20)$ dB.

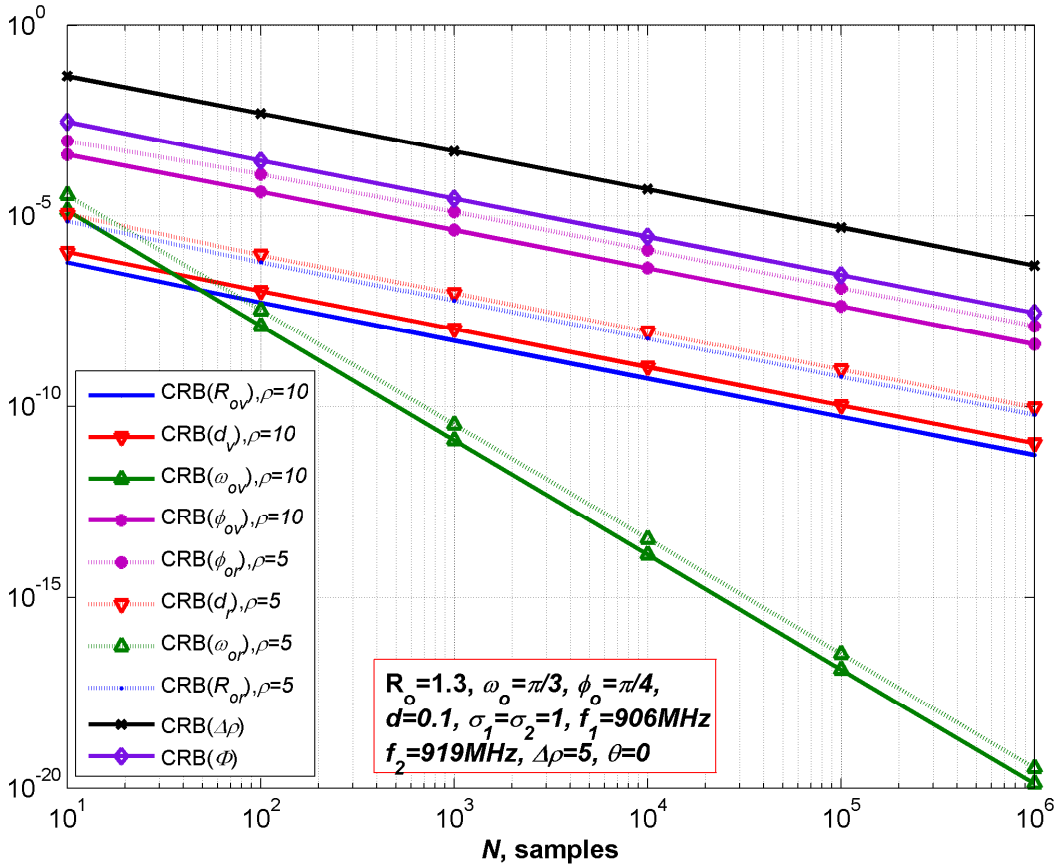
10^{0}
10^{-5}
10^{-10}
10^{-15}
10^{-20}
10^{1}
10^{2}
10^{3}
10^{4}
10^{5}
10^{6}
N, samples
CRB(R_{ov}),ρ=10
CRB(d_v),ρ=10
CRB(ω_{ov}),ρ=10
CRB(ϕ_{ov}),ρ=10
CRB(ϕ_{or}),ρ=5
CRB(d_r),ρ=5
CRB(ω_{or}),ρ=5
CRB(R_{or}),ρ=5
CRB($\Delta\rho$)
CRB(Φ)
R_o=1.3, ω_o=π/3, ϕ_o=π/4,
d=0.1, σ_1=σ_2=1, f_1=906MHz
f_2=919MHz, Δρ=5, θ=0

Fig.2. MD CRBs.

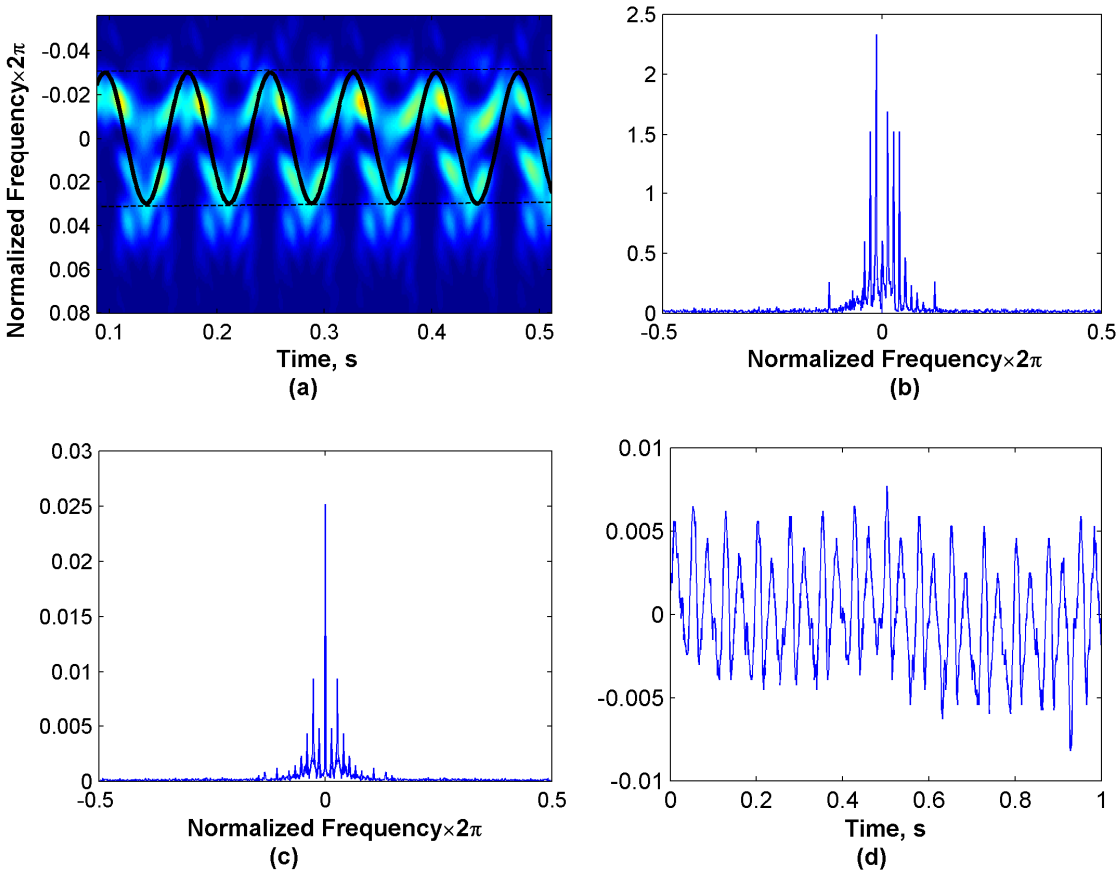

Fig. 3. (a) Spectrogram of the returns, (b) FFT of raw returns, (c) Second order cyclic moment.

(d) Real part of the returns.

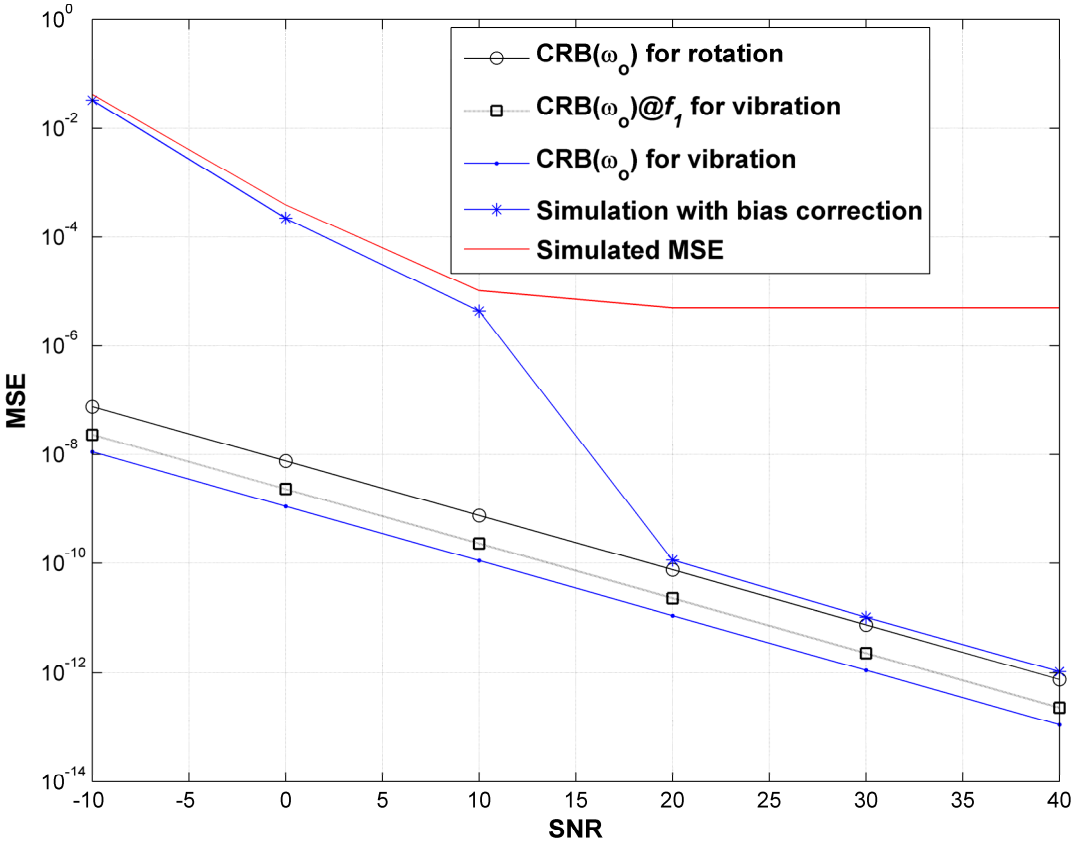

Fig. 4. Simulation results with respect to SNR.